Crystal structures of LeuT reveal conformational dynamics in the outward-facing states

Received for publication, February 23, 2021, and in revised form, March 23, 2021 Published, Papers in Press, April 1, 2021,
https://doi.org/10.1016/j.jbc.2021.100609

Jianjun Fan[1,‡], **Yang Xiao**[1,‡], **Matthias Quick**[2,3,‡], **Yuwei Yang**[1], **Ziyi Sun**[1,*], **Jonathan A. Javitch**[2,3,4,*], and **Xiaoming Zhou**[1,*]

From the [1]*Department of Integrated Traditional Chinese and Western Medicine, Rare Diseases Center, State Key Laboratory of Biotherapy, West China Hospital, Sichuan University, Chengdu, Sichuan, China;* [2]*Division of Molecular Therapeutics, New York State Psychiatric Institute,* [3]*Department of Psychiatry, Vagelos College of Physicians and Surgeons, and* [4]*Department of Pharmacology, Vagelos College of Physicians and Surgeons, Columbia University, New York, New York, USA*

Edited by Wolfgang Peti

The neurotransmitter:sodium symporter (NSS) homolog LeuT from *Aquifex aeolicus* has proven to be a valuable model for studying the transport mechanism of the NSS family. Crystal structures have captured LeuT in key conformations visited during the transport cycle, allowing for the construction of a nearly complete model of transport, with much of the conformational dynamics studied by computational simulations. Here, we report crystal structures of LeuT representing new intermediate conformations between the outward-facing open and occluded states. These structures, combined with binding and accessibility studies, reveal details of conformational dynamics that can follow substrate binding at the central substrate binding site (S1) of LeuT in outward-facing states, suggesting a potential competition for direction between the outward-open and outward-occluded states at this stage during substrate transport. Our structures further support an intimate interplay between the protonation state of Glu290 and binding of Na1 that may ultimately regulate the outward-open-to-occluded transition.

The neurotransmitter:sodium symporter (NSS) family, which includes the dopamine transporter (DAT) and the serotonin transporter (SERT), plays critical roles in regulating the temporal and spatial details of neurotransmission and has been implicated in the pathobiology and/or treatment of various neuropsychiatric disorders (1). LeuT from *Aquifex aeolicus* is a prokaryotic NSS homolog and an established model for dissecting the substrate binding and transport mechanism of the NSS family (2, 3). Studies have shown that LeuT mediates Na^+-dependent amino acid transport and contains two Na^+ binding sites, Na1 and Na2 (2). Unlike many eukaryotic NSS proteins that cotransport Cl^- with Na^+, LeuT counter-transports H^+ during its inward-to-outward return step, in which a key residue, Glu290, is thought to serve as the H^+ binding site (4, 5). To date, a number of crystal structures have been captured for LeuT, representing almost every key step along its transport cycle (Fig. 1) (2, 4, 6, 7), whereas the details of transitions between these conformations are mainly studied by molecular dynamics simulations (8–11).

Currently, three outward-facing conformations are available for LeuT: a H^+-bound outward-facing Na^+- and substrate-free return state (PDB entry 5JAE, Fig. 1*E*) (4), an outward-facing open state with Na1 and Na2 bound (PDB entry 3TT1, Fig. 1*A*) (7), and Na^+- and substrate-bound outward-facing occluded state (PDB entry 2A65, Fig. 1*B*) (2). To connect these three conformations in a forward transport cycle (Fig. 1), LeuT in the outward-facing return state (5JAE state, Fig. 1*E*) is thought to release its counter-transported H^+ (likely *via* Glu290 deprotonation) (5, 12), followed by binding of Na1 and Na2 (3TT1 state, Fig. 1*A*), succeeded by substrate binding at the central substrate-binding site (S1), eventually leading to the outward-facing occlusion (2A65 state, Fig. 1*B*). Substrate binding at a secondary substrate-binding site (S2) has been shown to promote the outward-occluded-to-inward transition (3). Although S2 binding may also affect the outward-open-to-occluded transition, the presence of detergent at the S2 site complicates the use of the crystal structures to address its role (13). Computational simulations also suggest that the transition from the outward-facing open-to-occluded state happens in the following sequence: (I) The first Na^+ binds at the Na1 site; (II) the second Na^+ binds at the Na2 site; (III) the substrate binds at the S1 site; (IV) the side chain of Phe253 rotates to adopt the *trans* χ_1 rotamer atop the bound substrate; (V) transmembrane segment 1b (TM1b) and 6a (TM6a) move toward TM3 and TM10 to occlude the substrate/Na^+ from the extracellular milieu (9). Here, we present new LeuT structures to provide experimental details that reveal conformational dynamics between the outward-facing open and occluded states, offering new insights into its transport process.

Results and discussion

A low pH captures a dual-conformation structure of LeuT that loses Na1

Interestingly, some of our LeuT crystals grown in a membranous lipidic cubic phase (LCP) captured dual conformations simultaneously in a single crystal (Fig. 2*A* and Table 1). These crystals emerged from a routine additive screen for

‡ These authors contributed equally to this work.
* For correspondence: Ziyi Sun, ziyi.sun@scu.edu.cn; Jonathan A. Javitch, jonathan.javitch@nyspi.columbia.edu; Xiaoming Zhou, x.zhou@scu.edu.cn.

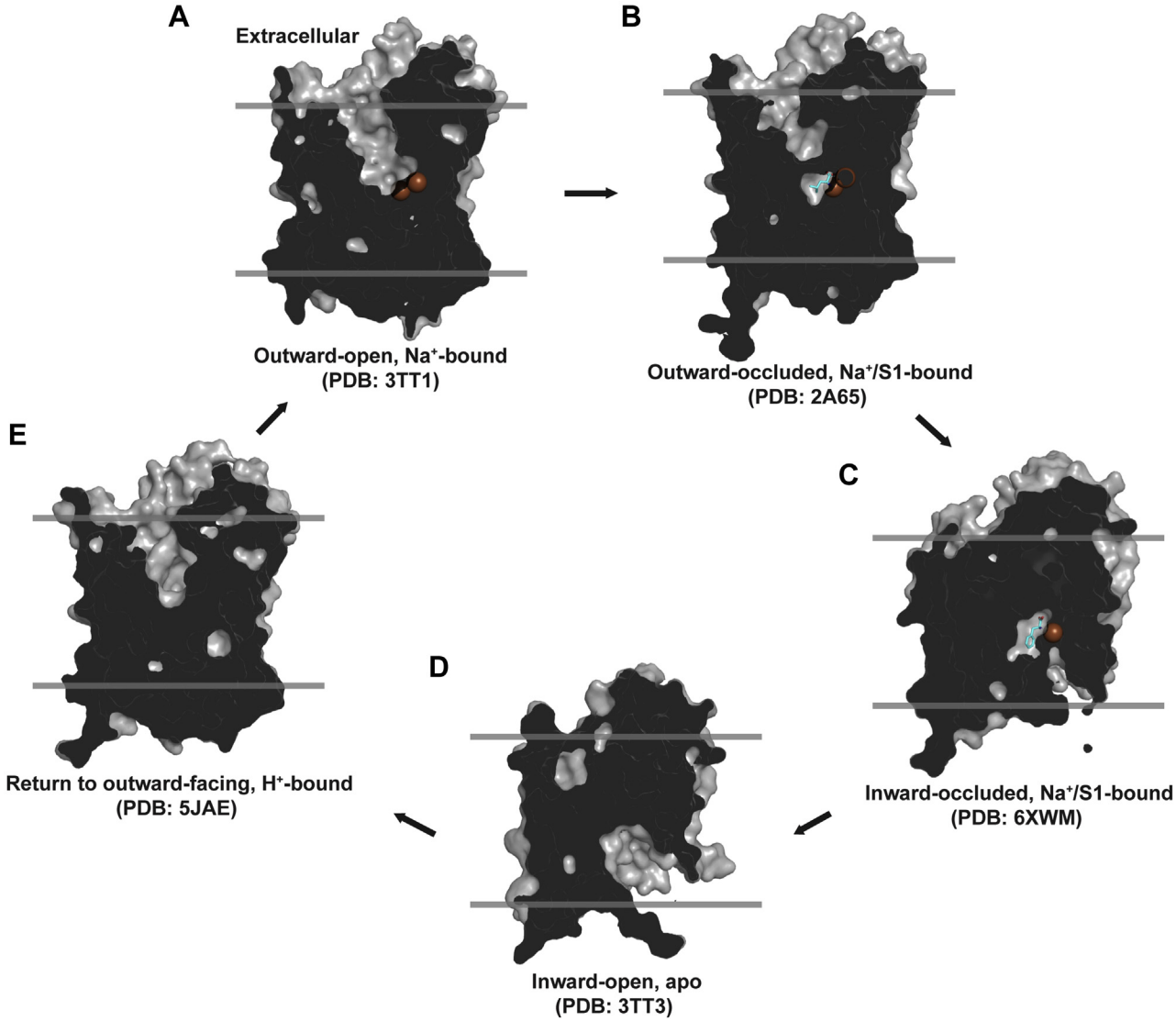

Figure 1. Illustration of the forward transport cycle of LeuT with known structures. A substrate is expected to bind to the primary site of LeuT in an outward-open state (*A*), leading the transporter to an outward-occluded state (*B*). LeuT then isomerizes to an inward-occluded state (*C*) and releases its substrate and Na^+ to assume an inward-open state (*D*), in which a counter-ion (H^+) is thought to bind. LeuT then isomerizes back to the outward-open state through an outward-facing return state (*E*), readying itself for the next transport cycle.

wild-type LeuT crystallized in LCP in the presence of Na^+/substrate, most of which yielded a 2A65-like outward-facing occluded structure with a TM-domain-Cα RMSD of 0.47 Å when aligned to the 2A65 structure (Fig. 2*B*). However, in the presence of the additive tris(2-carboxyethyl)phosphine hydrochloride (TCEP-HCl, unbuffered), LeuT crystallized in a dual-conformation state (Fig. 2*A*). One protomer (molecule A) closely resembles the outward-occluded 2A65 conformation with an all-Cα RMSD of 0.36 Å (TM-domain-Cα RMSD of 0.22 Å) to the 2A65 model and has one substrate (selenomethionine, SeMet) bound at the S1 site and two Na^+ bound at the Na1 and Na2 sites (Fig. 2*B*). In contrast, the other protomer (molecule B) is similar to the outward-open 3TT1 conformation, as the structural superposition of molecule B on the 3TT1 model yielded an all-Cα RMSD of 0.46 Å (TM-domain-Cα RMSD of 0.34 Å) (Fig. 2*C*), while it differs from molecule A (or the 2A65 model) by an all-Cα RMSD of ∼1.2 Å. However, molecule B and the 3TT1 structure differ in two important ways. First, substrate (SeMet) is bound at the S1 site with Phe253 adopting the *trans* χ_1 rotamer in molecule B while the 3TT1 structure is substrate-free with Phe253 in a *gauche* χ_1 rotamer (Fig. 2*C*), suggesting that the molecule B conformation occurs after the 3TT1 state as the Phe253 side chain has rotated to trap bound S1. Second, Na2, but not Na1, is bound in molecule B, as the simulated annealing F_o-F_c map (contoured at 3 σ level) that omits all Na^+ shows no electron density for Na1 in molecule B, but displays unambiguous and strong densities corresponding to Na2 in molecule B, as well as both Na1 and Na2 in molecule A (Fig. 2*D*). Since S1 is thought to bind after the binding of Na1 and Na2 (9), this result suggests that Na1 might be released after the bound S1 is trapped by Phe253 during the outward-open-to-occluded transition in LeuT.

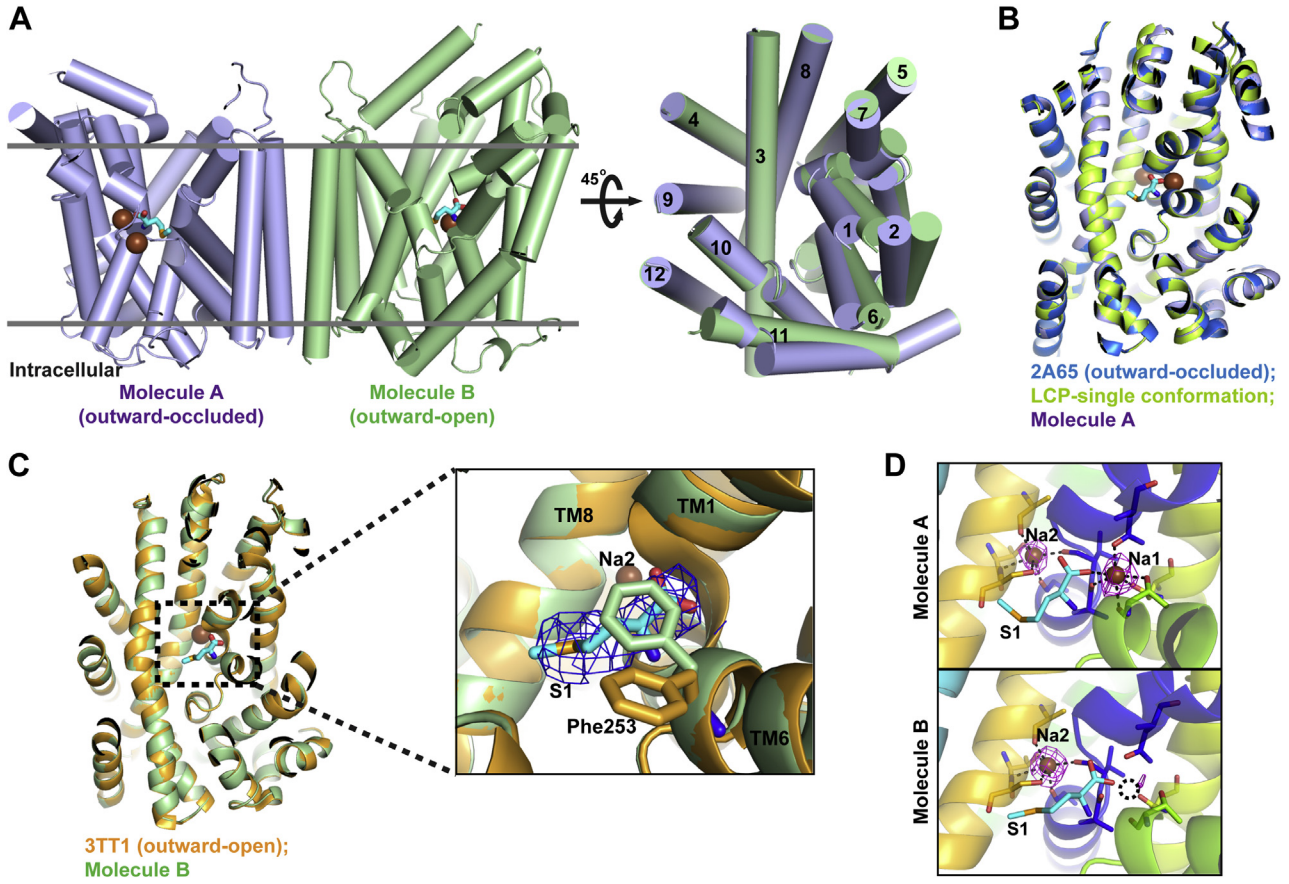

Figure 2. Dual-conformation structure of LeuT in lipidic cubic phase. *A*, the asymmetric unit contains two protomers of LeuT crystallized in lipidic cubic phase at pH 5.0 in the presence of Na^+/substrate. Molecule A is shown in cartoon cylinder mode in *light blue* and molecule B in *pale green*. The substrate (SeMet) is rendered as *cyan sticks* and Na^+ as *brown spheres* here and throughout this figure. The TM segments are numbered from 1 to 12 in the structural superposition of molecule B on molecule A. *B*, structural superposition of molecule A and the LeuT-LCP-single-conformation structure (pH 7.0) on the outward-occluded 2A65 structure. *C*, structural superposition of molecule B on the outward-open 3TT1 structure. Phe253 is shown in stick mode in the close-up view. The *blue mesh* shows the $2F_o$-F_c map contoured at 1.5 σ level with carve = 2. (d) The *purple mesh* shows the simulated annealing F_o-F_c omit map for Na^+ in molecule A (*upper panel*) and molecule B (*lower panel*), contoured at 3.0 σ level with carve = 2. Na^+-coordinating residues are displayed in *sticks*. A *black circle* with *dotted outline* is placed in the approximate position of the missing Na1 as if it was present for better indication of its location.

Since LeuT is naturally cysteine-free, the reducing power of TCEP-HCl is not expected to affect LeuT directly and thus cannot explain its impact on crystallization. Since unbuffered TCEP-HCl is a fairly strong acid, we hypothesized that TCEP led to the dual-conformation structure by acidifying the solution. Indeed, the pH of the dual-conformation crystallization solution was measured to be ∼5.0, compared with 7.0 for the single-conformation solution. This suggests that the acidic pH affected the LeuT protonation state, leading to a shift of its conformational distribution from a single-conformation state (occluded, pH 7.0) toward a dual-conformation equilibrium (open and occluded, pH ∼5.0) with both states captured during the LCP crystal formation and also may have caused release of Na1 in molecule B.

Low pH disrupts Na1 binding

To explore the effect of low pH on Na^+ binding, we measured $^{22}Na^+$ binding to wild-type LeuT as a function of pH (Fig. 3*A*). Interestingly, the maximal binding of $^{22}Na^+$ at pH ≤6.5 is approximately half of that ≥pH 7.5. Performing isotopic dilution of bound $^{22}Na^+$ at pH 5.5 and pH 8.0 revealed that the Hill coefficient is ∼1 at pH 5.5 compared with ∼2 at pH 8.0 (Fig. 3*B*). Although the Hill coefficient reflects cooperativity rather than the absolute number of binding sites, previous studies determined a Hill coefficient of 2 for Na^+ binding by LeuT (3) and two bound Na^+ are present in the crystal structure of LeuT (*e.g.*, 2A65). Consistently, a Hill coefficient of unity, as identified when the binding experiments were performed at pH 5.5, indicates a lack of cooperativity, which would be consistent with the binding of a single Na^+ to LeuT at pH 5.5, further suggesting that binding of either Na1 or Na2 is lost at low pH. $^{22}Na^+$ binding to LeuT-T354A (a Na2 mutant) decreased >80% at pH 5.5 compared with at pH 8.0, while $^{22}Na^+$ binding to LeuT-N27A (a Na1 mutant) only decreased slightly at the lower pH (Fig. 3*A*), indicating that Na1 binding is selectively disrupted at low pH (*e.g.*, pH 5.5). Using the method we devised previously to kinetically trap Na1 and S1 at neutral pH (3), we found that upon buffer change to pH 5.5, both S1 (Fig. 3*C*) and Na1 (Fig. 3*D*) were released, further supporting the hypothesis that low pH weakens Na1 binding, which in turn disrupts S1 binding. These data are consistent with the structure of molecule B in that Na1 is absent, but notably S1 remains trapped in the crystal structure, unlike in detergent where S1 release follows Na1 release.

Table 1
Data collection and refinement statistics of LeuT variant structures

PDB ID	LeuT-LCP-single 7DII	LeuT-LCP-dual 7DIX	LeuT-G26C 7DJ1	LeuT-G26C/E290S 7DJ2	LeuT-G26C/Q250A 7DJC
Data collection					
Space group	P 1	P 1 2_1 1	P 1 2_1 1	P 1 2_1 1	C 1 2 1
Wavelength (Å)	1.1	0.979	0.9792	0.9792	0.9792
Unit cell					
a, b, c (Å)	64.59, 72.18, 80.81	74.16, 115.07, 80.82	81.85, 94.12, 94.25	82.33, 110.71, 87.14	90.76, 87.61, 81.81
α, β, γ (°)	100.9, 97.6, 115.2	90, 102.9, 90	90, 95.9, 90	90, 96.0, 90	90, 94.3, 90
Resolution (Å)	2.40 (2.49–2.40)	3.49 (3.62–3.49)	3.53 (3.65–3.53)	2.40 (2.49–2.40)	2.70 (2.80–2.70)
Unique reflections	47,538 (4722)	16,444 (1655)	17,499 (1729)	60,623 (6030)	17,462 (1730)
Multiplicity	3.5 (3.0)	3.0 (3.0)	3.4 (3.5)	3.4 (3.3)	3.4 (3.2)
Completeness (%)	96.79 (96.13)	96.80 (98.22)	98.02 (98.00)	99.64 (99.59)	98.80 (98.13)
I/σI	11.91 (2.39)	8.15 (2.25)	7.01 (1.96)	7.18 (1.75)	14.01 (2.39)
R_{merge}	0.069 (0.436)	0.141 (0.597)	0.143 (0.698)	0.124 (0.618)	0.093 (0.623)
R_{meas}	0.082 (0.534)	0.170 (0.717)	0.170 (0.822)	0.147 (0.739)	0.111 (0.749)
R_{pim}	0.043 (0.302)	0.094 (0.393)	0.091 (0.431)	0.078 (0.402)	0.060 (0.412)
$CC_{1/2}$	0.997 (0.875)	0.993 (0.773)	0.996 (0.822)	0.994 (0.765)	0.997 (0.797)
Refinement					
Resolution (Å)	2.40 (2.45–2.40)	3.49 (3.71–3.49)	3.53 (3.71–3.53)	2.40 (2.44–2.40)	2.70 (2.84–2.70)
No. reflections	47,485 (4721)	16,391 (1654)	17,367 (1719)	60,578 (6027)	17,440 (1728)
Completeness (%)	96.5	97.2	98.6	98.7	98.6
R_{work}/R_{free} (%)	19.3/21.4	22.1/25.0	24.7/27.3	21.2/23.9	20.8/24.2
No. atoms	7934	7909	7788	8121	3911
Protein	7821	7882	7766	7854	3874
Ligands	22	21	22	60	31
Solvent	91	6		207	6
Average B-factor	50.96	61.44	83.23	44.90	63.69
Protein	50.92	61.46	83.24	44.73	63.62
Ligands	37.70	46.00	74.54	62.24	79.61
Solvent	55.17	47.48		47.82	49.22
Ramachandran plot					
Favored (%)	98.45	98.06	98.03	97.75	98.12
Allowed (%)	1.55	1.94	1.97	2.25	1.88
Outliers (%)	0.00	0.00	0.00	0.00	0.00
RMS bonds (Å)	0.002	0.002	0.003	0.002	0.002
RMS angles (°)	0.454	0.489	0.485	0.493	0.505

Statistics for the highest-resolution shell are shown in parentheses.
Table contents generated by phenix.table_one (30).

Protonation state of Glu290 affects outward opening of LeuT

Previous studies indicate that the protonation state of a single residue Glu290 (gain/loss of negative charge) is critical for regulating Na^+ binding at the Na1 site and a nearby Na1′ site (8), as well as the inward-to-outward transition of LeuT, by serving as the binding site for the counter-transported proton (4, 5). We, therefore, tested if Glu290 is involved in the aforementioned low-pH effect that promoted the outward-open conformation for LeuT seen in molecule B (the "low-pH" effect). To do so, we introduced a cysteine mutation (G26C) in LeuT to monitor its outward-openness by measuring the reactivity of a membrane-impermeant, thiol-modifying (PEGylating) agent, methoxypolyethylene glycol maleimide 5000 (mPEG-Mal-5K), from the extracellular milieu (14). Structural comparison shows that residue 26 is more accessible to mPEG-Mal-5K modification in the molecule B structure (open state) than in the molecule A structure (occluded state) in which the solvent-access path from the extracellular side to this position is narrowed (Fig. 4, *A* and *B*). We hypothesized, therefore, that acidic pH would promote an outward-open conformation with increased accessibility to modification of G26C by mPEG-Mal-5K, resulting in a 5 kDa shift in its molecular weight on SDS-PAGE. Consistent with this prediction, when *E. coli* cells expressing LeuT-G26C were incubated with mPEG-Mal-5K in the presence of Na^+/substrate, PEGylation was enhanced at pH 5.0 (Fig. 4, *C* and *D*), despite the fact that the thiol-modification reaction rate is slower at pH 5.0 compared with pH 8.0 (15). This result indicates that LeuT-G26C is substantially more outward-open at pH 5.0 than at pH 8.0, more than compensating for the slower PEGylation rate at the lower pH. We next mutated Glu290 to serine (E290S) in LeuT-G26C and repeated the PEGylation experiment. The "low-pH" effect was lost in the double mutant of LeuT-G26C/E290S, as the pH 5.0 condition yielded the least PEGylation and pH 8.0 the most (Fig. 4, *C* and *D*), likely due to the underlying effect of pH on modification rates (15). These data strongly indicate that Glu290 plays a pivotal role in mediating the "low-pH" effect, likely through protonation of its side chain carboxyl group. Consistent with this interpretation, the side chain carboxyl group of Glu290 in molecule B is accessible to the extracellular solvent from the S1 site (Fig. 4*E*).

LeuT structures reveal potential mechanism of Glu290 that regulates outward opening

Since a valid interpretation of these accessibility results relies on the structural integrity of LeuT-G26C and LeuT-G26C/E290S, we crystallized these mutant proteins at ∼pH 7 and solved their structures (Table 1). The two structures are almost identical in the main-chain organization as their all-Cα RMSD is only 0.22 Å, and both structures assumed a conformation similar to the wild-type 2A65 structure (occluded with S1) with a TM-domain-Cα RMSD of ∼0.54 Å (Fig. 5*A*). Thus, the G26C and E290S mutations did not perturb the structural integrity of LeuT or its ability to bind substrate. Also, as

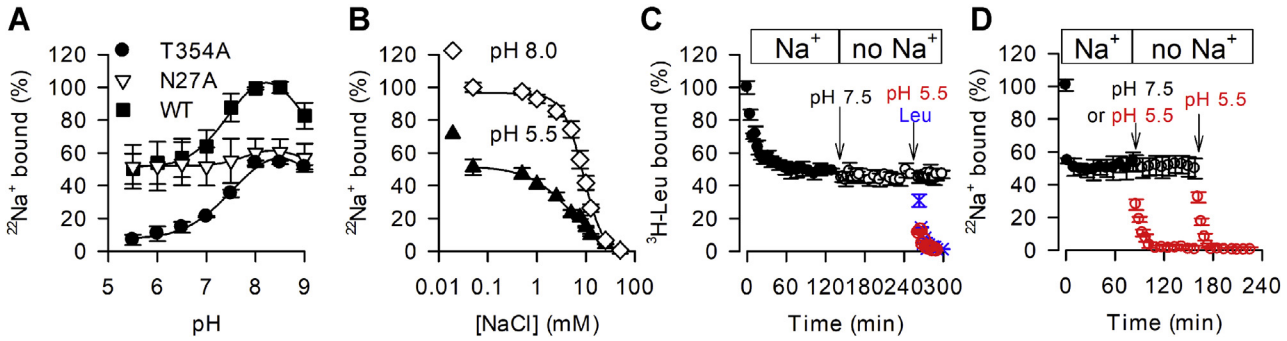

Figure 3. Na1 binding is disrupted by H^+. *A*, pH dependence of [^{22}Na]Cl binding by LeuT variants. Binding of 1 μM [^{22}Na]Cl was assayed with 50 ng of LeuT-WT, -N27A (Na1 site mutant), or -T354A (Na2 site mutant) using the SPA by varying the pH of the assay buffer from pH 5.5 to 9.0. *B*, effect of pH on the LeuT-WT Na^+ binding concentration dependence. Isotopic replacement of 1 μM [^{22}Na]Cl at pH 8.0 and pH 5.5 revealed $EC_{50}^{Na^+}$ values of 8.78 ± 0.47 mM and 5.22 ± 0.70 mM, respectively, and Hill coefficients of 2.07 ± 0.23 and 0.97 ± 0.13, respectively. Data in *panels A* and *B* are shown as mean ± SEM of three independent measurements and normalized with respect to the activity measured at pH 8.0. Nonlinear regression in SigmaPlot 13 was used to fit the isotherms, and the best-fit values of the $EC_{50}^{Na^+}$ and the Hill slope are represented as the mean ± SEM of the fit. *C*, dissociation of Leu trapped in the S1 site of LeuT-WT. Dissociation of 100 nM ^{3}H-Leu after 16-h incubation in the presence of 50 mM NaCl by dilution in assay buffer containing only 50 mM NaCl (Na^+ box) followed by subsequent dilution (*arrow*) into Na^+-free buffer (no Na^+ box) at pH 7.5 (O) and then (as indicated by *arrow*) into Na^+-free buffer at pH 5.5 (○). Release of trapped Leu in the S1 site induced by the addition of 1 μM Leu in Na^+-free buffer at pH 7.5 (x) served as control (3). *D*, dissociation of Na^+ trapped in the Na1 site in LeuT-WT. Dissociation of 1 μM [$^{22}Na^+$] after 16-h incubation in the presence of 100 nM Leu by dilution into buffer containing only 50 mM NaCl (Na^+ box), followed by the dilution (*arrow*) of the sample in Na^+-free buffer (no Na^+ box) at pH 5.5 (○) or pH 7.5 (O) that was followed by dilution (*arrow*) into Na^+-free buffer at pH 5.5 (○). *Panels C* and *D* show representative experiments that were repeated three times, and error bars indicate the mean ± SEM of triplicates.

expected, while the sulfhydryl group of G26C points toward the solvent-access path, the solvent path is sufficiently narrow, with a chokepoint of ∼6.0 Å above the sulfhydryl in the outward-occluded conformation, which the maleimide group (∼6.5 Å wide) of mPEG-Mal-5K cannot pass (Fig. 5*B*). In contrast, G26C is much more accessible to the extracellular solvent in the outward-open state, with the width of the solvent-access path >10 Å (Fig. 5*C*). This result also confirms the structural basis for the differential PEGylation of G26C in LeuT in the outward-facing open and occluded states from the extracellular side.

Interestingly, Phe253 in both the LeuT-G26C and LeuT-G26C/E290S structures (occluded 2A65-like) adopts a *gauche* χ_1 rotamer even though S1 is bound (Fig. 5*D*), likely due to steric clash between the engineered Cys26 side chain and Phe253 in the *trans* χ_1 rotamer in these two structures. This configuration of Phe253 is similar to the outward-open 3TT1 conformation and would grant extracellular solvent access to the S1 site of LeuT in an outward-occluded state with S1 bound (Fig. 5, *D* and *E*). Furthermore, the Glu290 protonation state could be affected by solvent penetration to the S1 site, as seen in molecule B (Fig. 4*E*). Therefore, these two structures suggest a plausible mechanism for Glu290 protonation after S1 binding.

Notably, although the G26C mutation seems to favor Phe253 in a *gauche* χ_1 rotamer as in 3TT1, it does not force LeuT to assume a 3TT1-like outward-open conformation. In other words, the G26C mutation does not prevent LeuT from sampling both the outward-open and outward-occluded states. While the effect of the mutation complicates reliance on the PEGylation assay as an exact quantitation of the ratio of the two outward-facing states in the wild-type transporter, it nonetheless provides a valuable qualitative readout of the pH effect on the outward-facing conformations.

Gln250 participates in the Glu290-mediated "low-pH" effect in LeuT

It has been proposed previously that the protonation state of Glu290 exerts its regulatory function through a continuous H-bond network that also involves Gln250 (12). To test if Gln250 also plays a part in the Glu290-mediated "low-pH" effect in LeuT, we extended our accessibility analysis to the double mutant of LeuT-G26C/Q250A at different pHs (5.0, 6.5 and 8.0) and observed a similar PEGylation pattern to LeuT-G26C/E290S, but with weaker modification intensities (Fig. 6, *A* and *B*). The structure of LeuT-G26C/Q250A closely resembles LeuT-G26C/E290S (Fig. 6*C*), with an all-Cα RMSD of 0.70 Å, showing an intact structural organization of LeuT-G26C/Q250A. This result suggests that the "low-pH" effect in LeuT is also mediated through Gln250, in addition to Glu290. It is also noteworthy that unlike the other two G26C mutant structures described above, Phe253 in the LeuT-G26C/Q250A structure adopts the *trans* χ1 rotamer as in 2A65, providing further evidence that the G26C mutation does not trap Phe253 in a specific rotamer, allowing the mutant construct to serve as a valid tool to monitor the relative "outward-openness" of LeuT by PEGylation.

Interplay between Na1 binding and Glu290 protonation regulates the outward-open-to-occluded transition in LeuT

Based on the above observations, we propose a dynamic and competitive process between the outward-facing open and occluded states during the LeuT transport cycle. After S1 binding, rotamer movement of Phe253 may still allow solvent penetration to Glu290, and protonation of the Glu290 side chain may occur, leading to loss of negative charge and dissociation of Na1, and ultimately promoting LeuT to assume an outward-open configuration as in molecule B (the "low-pH" effect) (Fig. 7*A*). On the other hand, Glu290 deprotonation (gain of negative charge) and Na1 binding occur in concert to

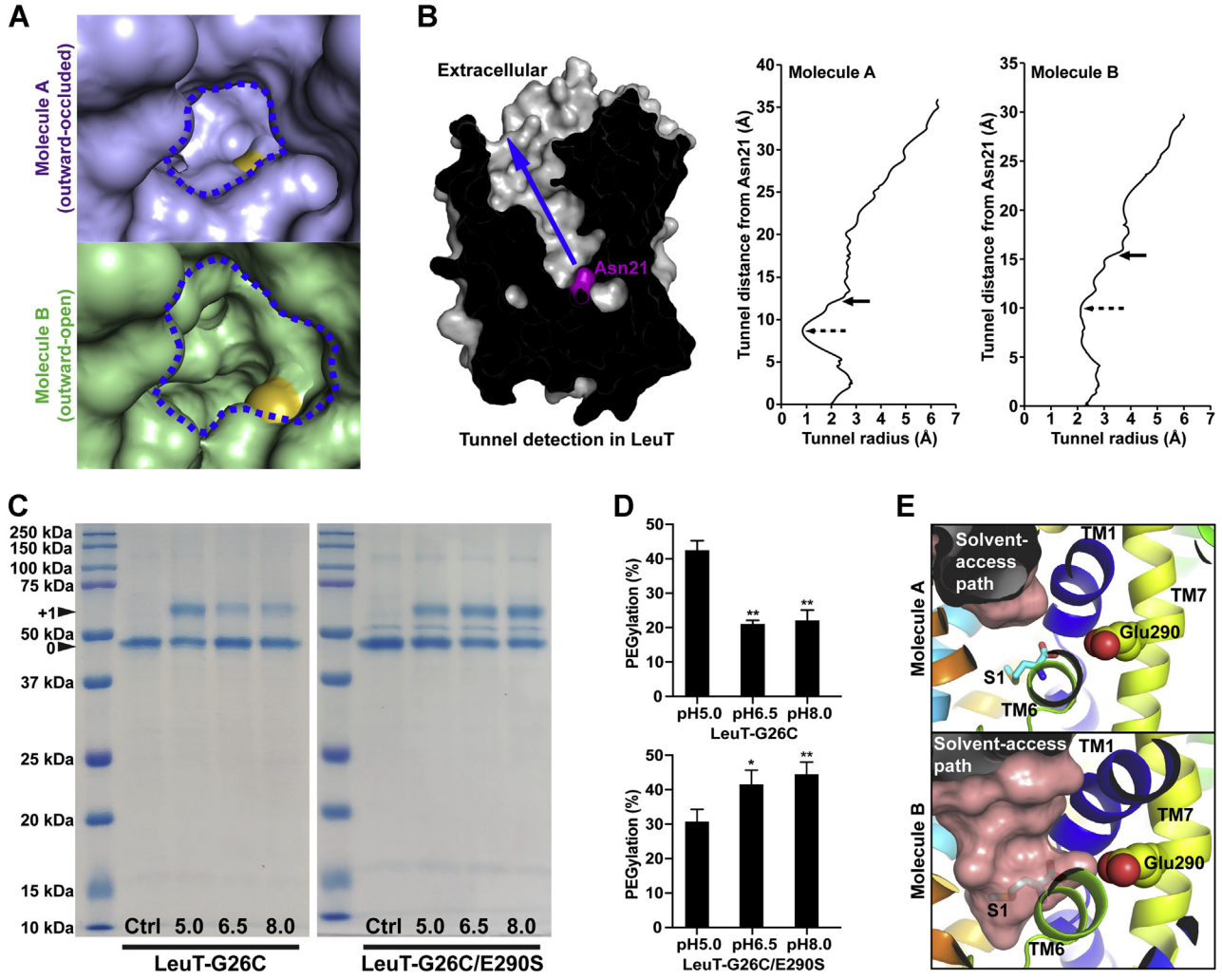

Figure 4. Cysteine accessibility of residue 26 of LeuT at different pHs. *A*, comparison of G26C accessibility between molecule A and molecule B shown in surface mode. The *gold* patch indicates the sulfhydryl group of the modeled G26C viewed from the extracellular side of LeuT. The "mouth" of the opening from the S1 site to the extracellular milieu is outlined by a *blue dashed line*. *B*, tunnel analysis by the MOLEonline 2.0 webserver for molecule A and B. The *left panel* shows the tunnel detection starting from Asn21 (colored in *magenta*) to the extracellular opening of LeuT (in *gray* surface representation), and the *blue arrow* indicates the tunnel direction. This setup was used throughout this study. The *middle* and *right panels* show the tunnel radius plot along the tunnel path for molecule A and B. The *dashed black arrow* indicates the bottleneck along the tunnel path, and the *solid black arrow* indicates the approximate position of residue 26. *C*, cell PEGylation of LeuT variants at different pHs (5.0, 6.5, 8.0) analyzed by SDS-PAGE as indicated. *Arrowheads* labeled with 0 and +1 indicate band positions without and with mPEG-Mal-5K modification. Protein markers indicate molecular weights of 10, 15, 20, 25, 37, 50, 75, 100, 150, and 250 kDa as shown from the bottom to the top of the gel. *D*, quantitation of results in (*C*) from independent experiments (n = 3). Data are expressed as mean ± SD. $^{*}p < 0.05$, $^{**}p < 0.01$. *E*, calculated solvent-accessible space of molecule A and molecule B from the extracellular side shown in *pink surface*. The side chain of Glu290 is shown in spheres and S1 in *sticks*.

push LeuT in the forward direction to the outward-occluded configuration as in molecule A (Fig. 7*A*). Consistent with this scheme, Na1 is also absent in the LeuT-G26C/E290S structure (Fig. 7*B*), because of the loss of a negative charge at the 290 position. Interestingly, in contrast to a previous structure of LeuT-E290S (12), we do not find Cl^- (or another anion) bound at this position to provide negative charge, which has been proposed to model Cl^- binding and dependence in many eukaryotic NSS proteins (16, 17). Whether this anion binding is prevented by simultaneous mutation of Gly26 is not yet clear, but both results are consistent with loss of Na1 binding at low pH due to loss of negative charge at this position. Notably, the pKa of the Glu290 side chain carboxyl group is calculated by PROPKA 3.1 to be 6.40 in molecule A and 5.85 in molecule B, suggesting that this proposed scenario may occur under physiological conditions as an adaptation to the extreme environmental conditions to which *A. aeolicus*, the native host of LeuT, is exposed. Whereas it has been generally accepted that the proton-motif force (pmf), consisting of the chemical H^+ transmembrane gradient ($\Delta\mu_{H^+}$) and the associated electrical potential across the membrane ($\Delta\Psi$), serves as energy source for many bacterial transport processes (18), the adaptation of *A. aeolicus* to its extreme habitat may involve respiratory flexibility that has been reported for a steadily increasing number of extremophilic prokaryotic organisms (19–21). It is possible that these conditions play a role in the regulation of the LeuT function by pH in its native environment.

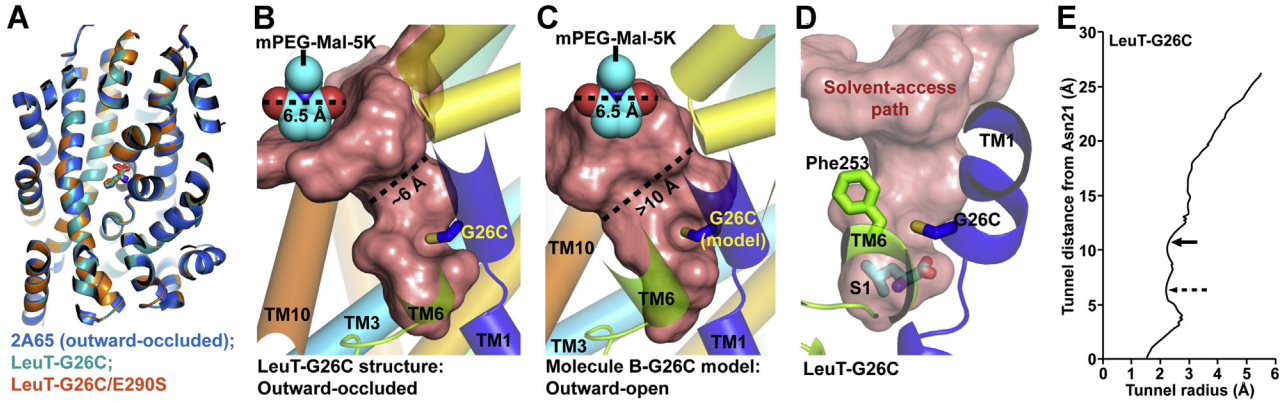

Figure 5. Crystal structures of LeuT-G26C and LeuT-G26C/E290S. *A*, structural superposition of LeuT-G26C and LeuT-G26C/E290S on the outward-occluded 2A65 structure. S1 is shown in *stick mode*. *B*, calculated solvent-accessible space of the LeuT-G26C structure from the extracellular side shown in *pink surface*. The G26C mutation is displayed in *sticks*, and the chokepoint of the solvent-access path above G26C is indicated by a *dashed line* (~6 Å long). An mPEG-Mal-5K molecule with its maleimide group rendered in *cyan spheres* is placed near the solvent-access path for better comparison. *C*, solvent-access analysis for the molecule B structure modeled with the G26C mutation, performed similarly as in *panel B*. *D*, extracellular solvent gains access to the S1 site in the LeuT-G26C structure. Phe253, G26C, and S1 are shown in *stick mode*. *E*, the tunnel radius plot along the tunnel path for LeuT-G26C analyzed by the MOLEonline 2.0 webserver. The *dashed black arrow* indicates the bottleneck (~2.2 Å radius here) along the tunnel path, which is larger than water (~1.4 Å radius), and the *solid black arrow* indicates the approximate position of the G26C mutation.

Furthermore, Na1 binding is thought to regulate the conformational dynamics as suggested in simulations and mutagenesis studies (8, 22). It was also proposed previously that a negative charge near Glu290, either from Glu290 deprotonation or a bound anion, connects to Na1 *via* Thr254 to regulate the extracellular gate Arg30-Asp404 *via* Gln250, forming an interaction network (12) that ultimately establishes the outward-occluded conformation. This notion is consistent with our dual-conformation structure. In molecule A, Glu290 (likely deprotonated) connects to Na1 and Gln250, allowing Arg30 to interact directly with Asp404 to stabilize the outward-occluded state (Fig. 6*D*), which can be described as: S1-$Na1^+$-Thr254-$Glu290^-$-Gln250 || $Arg30^+$-$Asp404^-$ ("-" indicates interaction while "||" indicates disruption of interaction) → outward-occluded. However, in molecule B, Glu290 (likely protonated) connects to Arg30 through Gln250 and promotes an outward-open conformation by preventing Arg30 from interacting with Asp404 (Fig. 6*E*), which can be described as: S1 || Thr254-Glu290 (neutral)-Gln250-$Arg30^+$ || $Asp404^-$ → outward-open. In addition, Na1 binding and Glu290 protonation also impact the Phe253 rotamer

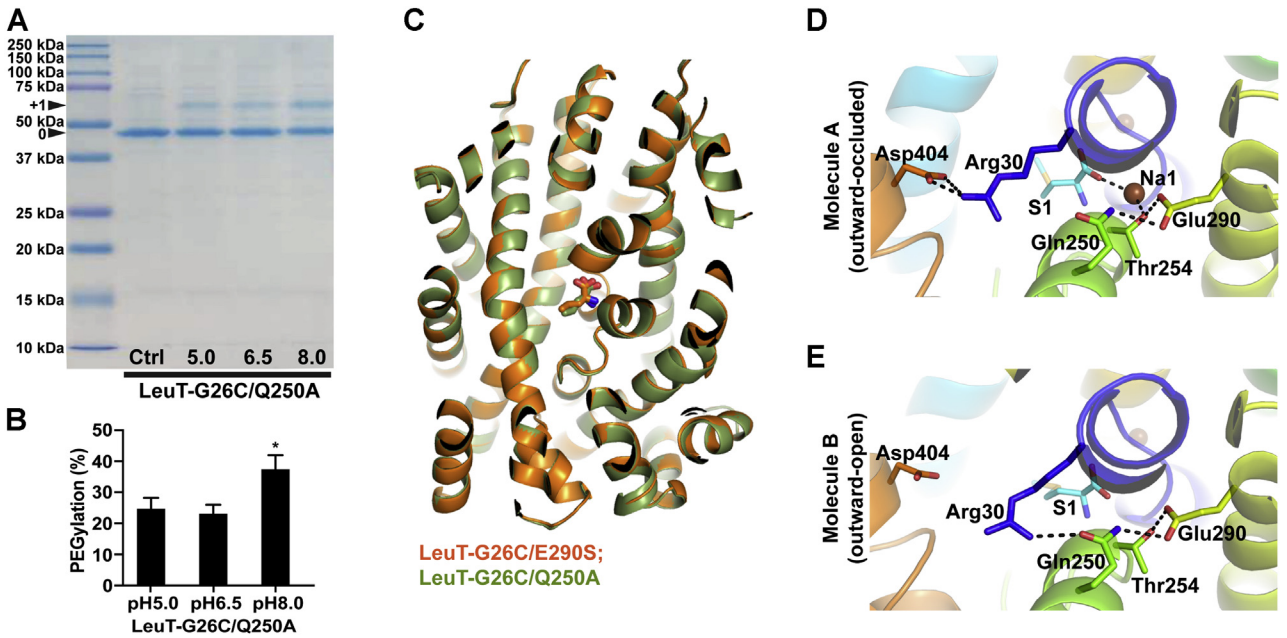

Figure 6. The Na1-Glu290-Gln250 interaction network regulates the outward-open-to-occluded transition in LeuT. *A*, cell PEGylation of LeuT-G26C/Q250A at different pHs (5.0, 6.5, 8.0) analyzed by SDS-PAGE as indicated. *Arrowheads* labeled with 0 and +1 indicate band positions without and with mPEG-Mal-5K modification. Protein markers indicate molecular weights of 10, 15, 20, 25, 37, 50, 75, 100, 150, and 250 kDa as shown from the bottom to the top of the gel. *B*, quantitation of results in (*A*) from independent experiments (n = 3). Data are expressed as mean ± SD. *$p < 0.05$. *C*, structural superposition of LeuT-G26C/Q250A on LeuT-G26C/E290S. S1 is shown in *sticks*. *D* and *E*, the Glu290-Gln250 interaction network that connects from S1 to the Arg30-Asp404 gate in molecule A (*panel D*) and molecule B (*panel E*). Engaging residues as well as S1 are displayed in *stick mode*. Na^+ is show in *brown spheres*. Interactions that constitute the network are indicated by *dashed lines*.

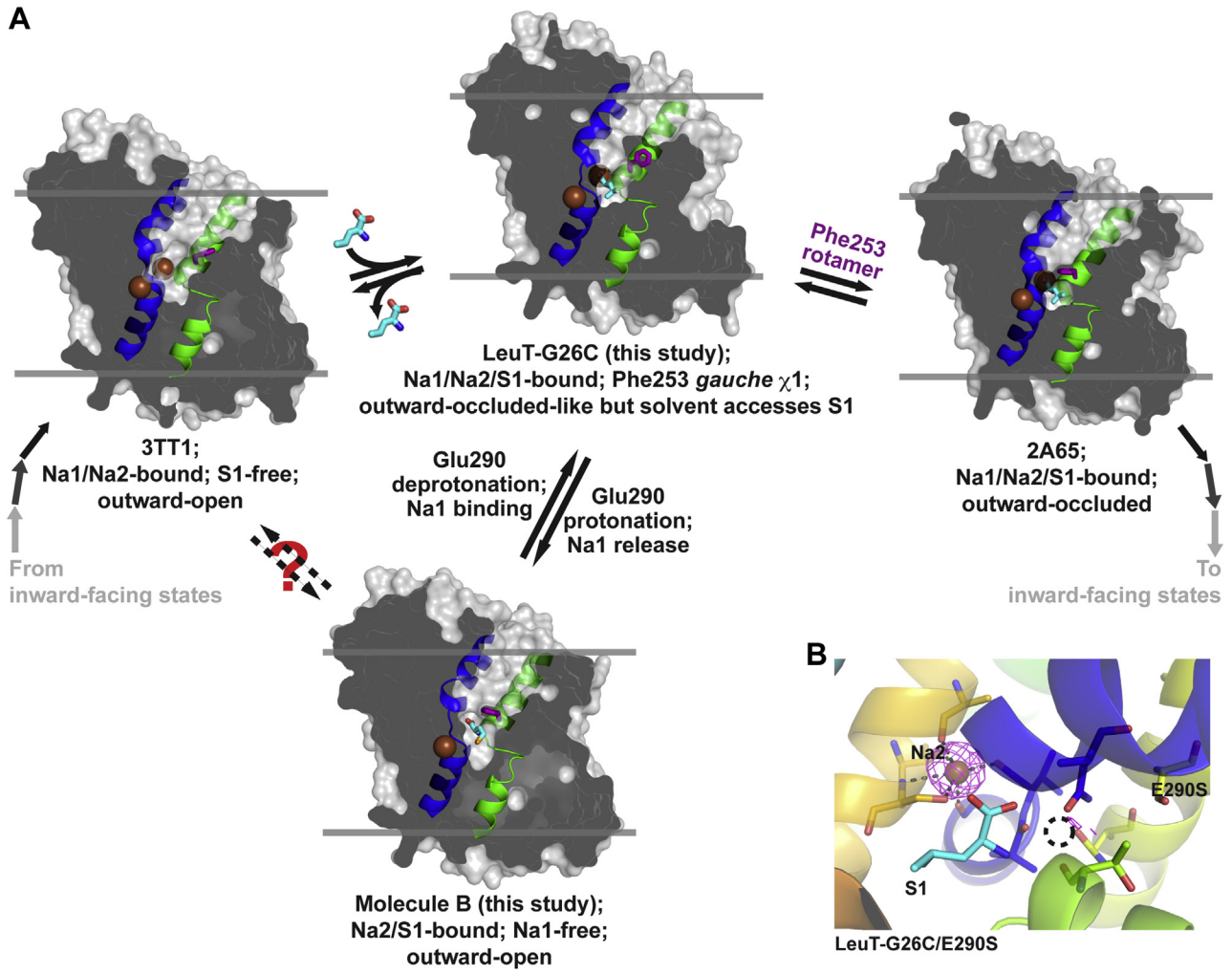

Figure 7. Conformational dynamics of the outward-facing states of LeuT in its transport cycle. *A*, an updated transport cycle of LeuT showing more conformational complexity between the outward-open and outward-occluded states by including the LeuT-G26C and molecule B structures. LeuT is displayed in *gray surface* with TM1 (*blue*) and TM6 (*green*) rendered in cartoon. Phe253 is shown in *purple sticks*, and S1 in *cyan sticks*. Na^+ is rendered in *brown spheres*. The *dashed arrows* and *red question mark* between 3TT1 and molecule B suggest possible conformational dynamics between these two states and that more work is needed to verify this process. *B*, the *purple mesh* shows the simulated annealing F_o-F_c omit map for Na^+ in the LeuT-G26C/E290S structure, contoured at 3.0 σ level with carve = 2. Na^+-coordinating residues are displayed in *sticks*. A *black circle* with *dotted outline* is placed in the approximate position of the missing Na1 as if it was present for better indication of its location.

position, which plays a critical role in regulating the outward-openness of LeuT. For example, the *trans* χ_1 rotamer of Phe253 is likely stabilized by two factors: binding of S1, and the cation–π interaction between Arg30 and Phe253. Through the interaction network described above, the presence of Na1 likely stabilizes S1 binding and promotes Arg30-Asp404 interaction, which positions Arg30 to interact with Phe253 in the *trans* χ_1 rotamer. Therefore, Glu290 protonation, which promotes Na1 dissociation, would affect both S1 stability and the Arg30 rotamer, which destabilize the *trans* χ_1 rotamer of Phe253 and allow more freedom for a *gauche* χ_1 rotamer.

Our proposed model highlights the role of Glu290 protonation/deprotonation and Na1 binding/unbinding in regulating conformational transitions between the outward-open and outward-occluded states of LeuT and reveals directional competition in this process that likely impacts transport efficiency (Fig. 7*A*). From a structural perspective, our data provide the first experimental evidence of the conformational dynamics during the outward-open-to-occluded transition of LeuT, as well as an intimate interplay between Na1 binding and Glu290 protonation, which is critical to understanding its substrate binding and transport mechanism.

Experimental procedures

Protein expression and purification

All LeuT mutations were introduced by QuikChange II system (Agilent) according to manufacturer's recommendation, using a pQO18 plasmid harboring the wild-type LeuT gene from *A. aeolicus* as template (3), and all mutations were verified by DNA sequencing. LeuT variants were overexpressed in *E. coli* BL21-Gold (DE3) cells by adding 0.25 mM isopropyl-β-D-thiogalactoside (IPTG) at OD_{600nm} of ∼0.8 and shaking at 20 °C for 18 h. Cell pellets were resuspended in Lysis Solution (LS) containing 20 mM Tris-HCl, pH 7.5, 150 mM NaCl, 10% (v/v) glycerol, and 1 mM

phenylmethanesulfonyl fluoride (PMSF) and lyzed by an ATS AH-1500 high-pressure homogenizer at 900 MPa. Protein was extracted by addition of n-dodecyl-β-D-maltopyranoside (DDM, Anatrace) to final 20 mM at 20 °C for 2 h, and the extraction mixture was centrifuged at 75,000*g* for 20 min at 4 °C. The supernatant was then loaded onto a cobalt metal affinity column, washed with 20-bed volume of LS containing 2 mM DDM and 40 mM imidazole, pH 8.0, and eluted with LS supplemented with 2 mM DDM and 250 mM imidazole, pH 8.0.

Crystallization

LeuT variants were purified and treated with tobacco etch virus (TEV) protease at a 50:1 ratio (LeuT:TEV, w/w) for 30 min at 20 °C to remove the N-terminal decahistidine tag. For LCP crystallization, wild-type LeuT was concentrated to ∼10 mg/ml and further purified by size-exclusion chromatography (SEC) in a buffer containing 150 mM NaCl, 20 mM Tris-HCl, pH 7.5, and 1 mM DDM. Peak fractions were pooled and concentrated to ∼50 mg/ml and mixed with 1-oleoyl-rac-glycerol (monoolein, Sigma-Aldrich) containing 5 mol% *E. coli* polar lipids (Avanti Polar Lipids) at a 2:3 (w/w) protein-to-lipid ratio using the twin-syringe mixing method (23). The protein–lipid mixture was then dispensed manually in ∼50 nl drops onto 96-well glass sandwich plates and overlaid with 1 μl of precipitant solution per drop. The LeuT-LCP-single-conformation crystals grew in 0.1 M NaCl, 0.1 M Na^+-Hepes, pH 7.0, 32% (v/v) PEG 350 monomethyl ether, and 1 mM L-leucine (Leu). The LeuT-LCP-dual-conformation crystals grew in 0.1 M NaCl, 0.1 M Na^+-Hepes, pH 7.0, 32% (v/v) PEG 350 monomethyl ether, 10 mM tris(2-carboxyethyl) phosphine hydrochloride (TCEP-HCl, unbuffered), and 1 mM L-selenomethionine (SeMet), resulting in the final solution at pH ∼5.0. Of note, LeuT LCP crystals grow extremely slowly and usually reach full-size in 2 months and were directly flash-frozen in liquid nitrogen without additional cryo-protection. For crystallization using vapor diffusion method, LeuT variants were concentrated to ∼10 mg/ml and further purified by SEC in a buffer containing 150 mM NaCl, 20 mM Tris-HCl, pH 7.5, and 40 mM n-octyl-β-D-glucoside (OG). Peak fractions were pooled and concentrated to ∼5 mg/ml, and crystallization was carried out in a sitting-drop setup at 20 °C. The LeuT-G26C crystals grew in 0.2 M choline chloride, 0.1 M Tris-HCl, pH 7.5, 14% (w/v) PEG 2000 monomethyl ether, 15% (v/v) glycerol, and 1 mM L-Leu. The LeuT-G26C/E290S crystals grew in 0.1 M Mg^{2+}-formate dihydrate, 0.1 M Na^+-MOPS, pH 7.0, 17% (w/v) PEG 3350, and 15% (v/v) glycerol. The LeuT-G26C/Q250A crystals grew in 0.05 M Li_2SO_4, 0.1 M glycine, pH 9.0, and 25% (v/v) PEG 400. These crystals usually grow to full size in 1 week and were directly flash-frozen in liquid nitrogen, except that the LeuT-G26C/Q250A crystals were cryo-protected by gradually raising PEG 400 to 38% (v/v) before being flash-frozen.

Data collection, structure solution and structural analysis

Diffraction data were collected on beamlines BL18U1 and BL19U1 (24) of National Facility for Protein Science in Shanghai (NFPS) at Shanghai Synchrotron Radiation Facility. The data were indexed, integrated, and scaled using the autoPROC pipeline package (Global Phasing Limited) (25), which includes XDS (26) and AIMLESS (CCP4 package) (27). The LeuT-LCP-dual-conformation structure was solved by molecular replacement with Phaser (28) using both the outward-occluded 2A65 and the outward-open 3TT1 structures as templates, while all other LeuT variant structures were solved by molecular replacement using 2A65 as a search model. Manual model building and refinement were carried out using Coot (29) and phenix.refine (30), and Molprobity (31) was used to monitor and improve protein geometry. The data collection and refinement statistics listed in Table 1 were generated by phenix.table_one (30) except the model geometry parameters (RMS bonds and angles), which appear to be mistakenly reported by phenix.table_one and therefore were manually recorded from phenix.refine. All structure figures and RMSD calculations were performed in PyMOL (Schrödinger, LLC). Computational accessibility analysis was performed using the volume-filling program HOLLOW (32) with default settings. Tunnel analysis for LeuT was performed using the MOLEonline 2.0 webserver (https://mole.upol.cz) (33) with default settings except the parameter of Interior Threshold was set to 1.4 Å.

Cysteine accessibility analysis

Accessibility of G26C on LeuT from the extracellular side was probed by cell PEGylation using a membrane-impermeable PEGylating reagent, methoxypolyethylene glycol maleimide 5000 (mPEG-Mal-5K, Sigma-Aldrich), as described previously (14). Briefly, 10 ml of *E. coli* cells expressing LeuT-G26C, LeuT-G26C/E290S, or LeuT-G26C/Q250A was harvested and washed three times with Buffer I containing 150 mM NaCl, 2 μM L-Leu and 20 mM buffers at different pHs (Na^+-citrate pH 5.0, Na^+-MES, pH 6.5 or Na^+-Hepes, pH 8.0). The cell pellets were then resuspended in 900 μl of Buffer I with 100 μl of mPEG-Mal-5K (freshly prepared stock) added to a final concentration of 1 mM, and the mixture was incubated at room temperature for 1 h with shaking. The PEGylation reaction was stopped by addition of β-mercaptoethanol to a final concentration of 10 mM, and cells were pelleted and washed three times with Buffer II containing 20 mM Tris-HCl, pH 7.5, 150 mM NaCl, 10% (v/v) glycerol, and 2 mM β-mercaptoethanol. Cells were then resuspended in 1 ml of Buffer II supplemented with 1 mM PMSF and lyzed by sonication, and membrane proteins were extracted by addition of 20 mM DDM at 20 °C for 2 h. Cell debris and insoluble material were cleared by centrifugation at 20,000*g* for 20 min at 4 °C, and the supernatant was mixed with 20 μl of cobalt affinity beads and incubated at 20 °C for 30 min. The beads were pelleted and washed with 1 ml of Buffer II containing 2 mM DDM and 40 mM imidazole, pH 8.0 for three times, and then analyzed by SDS-PAGE gels and Coomassie staining. To quantify the PEGylating ratio of the G26C variants of LeuT, modified and unmodified band intensities were quantitated individually using ImageJ software (NIH). Briefly, after image background correction, equal-sized boxes were drawn encompassing the bands of interest to obtain the entire area intensity, and the intensity peak of the

band of interest was analyzed. The PEGylating ratio of the G26C variants was evaluated by the following equation: PEGylation (%) = (modified band intensity)/(modified + unmodified band intensities) × 100. All PEGylation experiments were conducted in triplicate, and the quantitation data are presented as mean ± SD. Student's *t*-test was used for statistical analysis between the pH5.0 group and other pH groups.

Scintillation proximity assay

Radiotracer binding studies were performed by means of the scintillation proximity assay (SPA) using copper-coated PVT (for $^{22}Na^+$) or YSi (for ^{3}H-Leu) SPA beads to immobilize His-tagged LeuT-variants (3). Binding of 1 μM [^{22}Na]Cl (14.6 Ci/mmol, PerkinElmer) was performed with 0.8 pmol (about 50 ng) of purified protein per 100 μl-assay in buffer composed of 400 mM Tris/Mes at the indicated pH, 1 mM TCEP, 0.1% (w/v) DDM, and 20% glycerol. For isotopic $^{22}Na^+$ replacement studies, Tris/Mes was equimolarly replaced with NaCl to obtain the $EC_{50}^{Na^+}$. Binding isotherms of data means ± SEM of three independent experiments were subjected to nonlinear regression fitting in SigmaPlot 13, and the kinetic constants are shown as mean ± SEM of the fit. For the Leu dissociation experiments, binding of 100 nM ^{3}H-Leu (100 Ci/mmol, American Radiolabeled Chemicals, Inc) to 50 ng LeuT-WT in 150 mM Tris/Mes, pH 7.5, 50 mM NaCl, 1 mM TCEP, 0.1% (w/v) DDM, and 20% glycerol was measured for 16 h at 23 °C. The sample was washed and diluted in the same assay buffer lacking ^{3}H-Leu, followed by dilution in 200 mM Tris/Mes, pH 7.5, 1 mM TCEP, 0.1% (w/v) DDM, and 20% glycerol. Release of trapped ^{3}H-Leu from the S1 site was triggered by the addition of 1 μM Leu or by changing the pH of the assay buffer from pH 7.5 to pH 5.5. Similar to the ^{3}H-Leu dissociation experiments, binding of 1 μM [^{22}Na]Cl to LeuT-WT for 16 h in 200 mM Tris/Mes, pH 7.5, 1 mM TCEP, 0.1% (w/v) DDM, 20% glycerol, and 100 nM Leu was followed by dilution of the sample in 150 mM Tris/Mes, pH 7.5, 50 mM NaCl, 1 mM TCEP, 0.1% (w/v) DDM, and 20% glycerol in the absence of $^{22}Na^+$. The sample was then subsequentially diluted into 200 mM Tris/Mes, 1 mM TCEP, 0.1% (w/v) DDM, and 20% glycerol at the indicated pH. For all functional assays, equal protein concentrations were used as determined with the amido black protein assay (34).

Data availability

The atomic coordinates and structure factors of all LeuT variant structures reported in this study were deposited in the Protein Data Bank under accession code 7DII (LeuT-LCP-single-conformation), 7DIX (LeuT-LCP-dual-conformation), 7DJ1 (LeuT-G26C), 7DJ2 (LeuT-G26C/E290S), and 7DJC (LeuT-G26C/Q250A).

Acknowledgments—Diffraction data used for this study were collected on beamlines BL18U1 and BL19U1 of National Facility for Protein Science in Shanghai (NFPS) at Shanghai Synchrotron Radiation Facility (SSRF). The authors thank the staff from these beamlines for assistance during data collection.

Author contributions—X. Z., Z. S., M. Q., and J. A. J. conceived the project. X. Z., Z. S., and J. A. J. wrote the article with input from all the authors. J. F. and Y. X. performed protein crystallization and data collection. J. F., Y. X., M. Q., and Y. Y. performed the functional studies. X. Z. and Z. S. solved structures and performed computational analysis. All the authors analyzed the data.

Funding and additional information—This work was supported in part by the National Natural Science Foundation of China grant No. 31770783 to X. Z., National Institutes of Health grant R01 DA041510 to JAJ, and R01 GM119396 to M. Q. The content is solely the responsibility of the authors and does not necessarily represent the official views of National Institutes of Health.

Conflict of interest—The authors declare that they have no conflicts of interest with the contents of this article.

Abbreviations—The abbreviations used are: DAT, dopamine transporter; DDM, n-dodecyl-β-D-maltopyranoside; LCP, lipidic cubic phase; LS, lysis solution; NSS, neurotransmitter:sodium symporter; OG, n-octyl-β-D-glucoside; PMSF, phenylmethanesulfonyl fluoride; SEC, size-exclusion chromatography; SERT, serotonin transporter; TCEP-HCl, tris(2-carboxyethyl)phosphine hydrochloride; TEV, tobacco etch virus.

References

1. Kristensen, A. S., Andersen, J., Jorgensen, T. N., Sorensen, L., Eriksen, J., Loland, C. J., Stromgaard, K., and Gether, U. (2011) SLC6 neurotransmitter transporters: Structure, function, and regulation. *Pharmacol. Rev.* **63**, 585–640
2. Yamashita, A., Singh, S. K., Kawate, T., Jin, Y., and Gouaux, E. (2005) Crystal structure of a bacterial homologue of Na^+/Cl^- dependent neurotransmitter transporters. *Nature* **437**, 215–223
3. Shi, L., Quick, M., Zhao, Y., Weinstein, H., and Javitch, J. A. (2008) The mechanism of a neurotransmitter:sodium symporter–inward release of NA^+ and substrate is triggered by substrate in a second binding site. *Mol. Cell* **30**, 667–677
4. Malinauskaite, L., Said, S., Sahin, C., Grouleff, J., Shahsavar, A., Bjerregaard, H., Noer, P., Severinsen, K., Boesen, T., Schiott, B., Sinning, S., and Nissen, P. (2016) A conserved leucine occupies the empty substrate site of LeuT in the Na^+-free return state. *Nat. Commun.* **7**, 11673
5. Zhao, Y., Quick, M., Shi, L., Mehler, E. L., Weinstein, H., and Javitch, J. A. (2010) Substrate-dependent proton antiport in neurotransmitter:sodium symporters. *Nat. Chem. Biol.* **6**, 109–116
6. Gotfryd, K., Boesen, T., Mortensen, J. S., Khelashvili, G., Quick, M., Terry, D. S., Missel, J. W., LeVine, M. V., Gourdon, P., Blanchard, S. C., Javitch, J. A., Weinstein, H., Loland, C. J., Nissen, P., and Gether, U. (2020) X-ray structure of LeuT in an inward-facing occluded conformation reveals mechanism of substrate release. *Nat. Commun.* **11**, 1005
7. Krishnamurthy, H., and Gouaux, E. (2012) X-ray structures of LeuT in substrate-free outward-open and apo inward-open states. *Nature* **481**, 469–474
8. Zhao, C., Stolzenberg, S., Gracia, L., Weinstein, H., Noskov, S., and Shi, L. (2012) Ion-controlled conformational dynamics in the outward-open transition from an occluded state of LeuT. *Biophys. J.* **103**, 878–888
9. Zomot, E., Gur, M., and Bahar, I. (2015) Microseconds simulations reveal a new sodium-binding site and the mechanism of sodium-coupled substrate uptake by LeuT. *J. Biol. Chem.* **290**, 544–555
10. Cheng, M. H., and Bahar, I. (2013) Coupled global and local changes direct substrate translocation by neurotransmitter-sodium symporter ortholog LeuT. *Biophys. J.* **105**, 630–639

11. Khelashvili, G., Schmidt, S. G., Shi, L., Javitch, J. A., Gether, U., Loland, C. J., and Weinstein, H. (2016) Conformational dynamics on the extracellular side of LeuT controlled by Na^+ and K^+ ions and the protonation state of Glu290. *J. Biol. Chem.* **291**, 19786–19799
12. Kantcheva, A. K., Quick, M., Shi, L., Winther, A. M., Stolzenberg, S., Weinstein, H., Javitch, J. A., and Nissen, P. (2013) Chloride binding site of neurotransmitter sodium symporters. *Proc. Natl. Acad. Sci. U. S. A.* **110**, 8489–8494
13. Quick, M., Winther, A. M., Shi, L., Nissen, P., Weinstein, H., and Javitch, J. A. (2009) Binding of an octylglucoside detergent molecule in the second substrate (S2) site of LeuT establishes an inhibitor-bound conformation. *Proc. Natl. Acad. Sci. U. S. A.* **106**, 5563–5568
14. Zhou, X., Levin, E. J., Pan, Y., McCoy, J. G., Sharma, R., Kloss, B., Bruni, R., Quick, M., and Zhou, M. (2014) Structural basis of the alternating-access mechanism in a bile acid transporter. *Nature* **505**, 569–573
15. Partis, M. D., Griffiths, D. G., Roberts, G. C., and Beechey, R. B. (1983) Cross-linking of protein by co-maleimido alkanoyl N-hydroxysuccinimido esters. *J. Protein Chem.* **2**, 263–277
16. Forrest, L. R., Tavoulari, S., Zhang, Y. W., Rudnick, G., and Honig, B. (2007) Identification of a chloride ion binding site in Na^+/Cl^- dependent transporters. *Proc. Natl. Acad. Sci. U. S. A.* **104**, 12761–12766
17. Zomot, E., Bendahan, A., Quick, M., Zhao, Y., Javitch, J. A., and Kanner, B. I. (2007) Mechanism of chloride interaction with neurotransmitter: sodium symporters. *Nature* **449**, 726–730
18. Kaback, H. R. (2015) A chemiosmotic mechanism of symport. *Proc. Natl. Acad. Sci. U. S. A.* **112**, 1259–1264
19. Kracke, F., Vassilev, I., and Kromer, J. O. (2015) Microbial electron transport and energy conservation - the foundation for optimizing bioelectrochemical systems. *Front. Microbiol.* **6**, 575
20. Conley, B. E., Weinstock, M. T., Bond, D. R., and Gralnick, J. A. (2020) A hybrid extracellular electron transfer pathway enhances the survival of Vibrio natriegens. *Appl. Environ. Microbiol.* **86**
21. Richardson, D. J. (2000) Bacterial respiration: A flexible process for a changing environment. *Microbiology (Reading)* **146**(Pt 3), 551–571
22. Tavoulari, S., Margheritis, E., Nagarajan, A., DeWitt, D. C., Zhang, Y. W., Rosado, E., Ravera, S., Rhoades, E., Forrest, L. R., and Rudnick, G. (2016) Two Na^+ sites control conformational change in a neurotransmitter transporter homolog. *J. Biol. Chem.* **291**, 1456–1471
23. Caffrey, M., and Cherezov, V. (2009) Crystallizing membrane proteins using lipidic mesophases. *Nat. Protoc.* **4**, 706–731
24. Zhang, W. Z., Tang, J. C., Wang, S. S., Wang, Z. J., Qin, W. M., and He, J. H. (2019) The protein complex crystallography beamline (BL19U1) at the Shanghai Synchrotron Radiation Facility. *Nucl. Sci. Tech.* **30**, 170–181
25. Vonrhein, C., Flensburg, C., Keller, P., Sharff, A., Smart, O., Paciorek, W., Womack, T., and Bricogne, G. (2011) Data processing and analysis with the autoPROC toolbox. *Acta Crystallogr. D Biol. Crystallogr.* **67**, 293–302
26. Kabsch, W. (2010) Xds. *Acta Crystallogr. D Biol. Crystallogr.* **66**, 125–132
27. Winn, M. D., Ballard, C. C., Cowtan, K. D., Dodson, E. J., Emsley, P., Evans, P. R., Keegan, R. M., Krissinel, E. B., Leslie, A. G., McCoy, A., McNicholas, S. J., Murshudov, G. N., Pannu, N. S., Potterton, E. A., Powell, H. R., *et al.* (2011) Overview of the CCP4 suite and current developments. *Acta Crystallogr. D Biol. Crystallogr.* **67**, 235–242
28. McCoy, A. J., Grosse-Kunstleve, R. W., Adams, P. D., Winn, M. D., Storoni, L. C., and Read, R. J. (2007) Phaser crystallographic software. *J. Appl. Crystallogr.* **40**, 658–674
29. Emsley, P., and Cowtan, K. (2004) Coot: Model-building tools for molecular graphics. *Acta Crystallogr. D Biol. Crystallogr.* **60**, 2126–2132
30. Afonine, P. V., Grosse-Kunstleve, R. W., Echols, N., Headd, J. J., Moriarty, N. W., Mustyakimov, M., Terwilliger, T. C., Urzhumtsev, A., Zwart, P. H., and Adams, P. D. (2012) Towards automated crystallographic structure refinement with phenix.refine. *Acta Crystallogr. D Biol. Crystallogr.* **68**, 352–367
31. Davis, I. W., Leaver-Fay, A., Chen, V. B., Block, J. N., Kapral, G. J., Wang, X., Murray, L. W., Arendall, W. B., 3rd, Snoeyink, J., Richardson, J. S., and Richardson, D. C. (2007) MolProbity: All-atom contacts and structure validation for proteins and nucleic acids. *Nucleic Acids Res.* **35**, W375–W383
32. Ho, B. K., and Gruswitz, F. (2008) Hollow: Generating accurate representations of channel and interior surfaces in molecular structures. *BMC Struct. Biol.* **8**, 49
33. Pravda, L., Sehnal, D., Tousek, D., Navratilova, V., Bazgier, V., Berka, K., Svobodova Varekova, R., Koca, J., and Otyepka, M. (2018) MOLEonline: A web-based tool for analyzing channels, tunnels and pores (2018 update). *Nucleic Acids Res.* **46**, W368–W373
34. Schaffner, W., and Weissmann, C. (1973) A rapid, sensitive, and specific method for the determination of protein in dilute solution. *Anal. Biochem.* **56**, 502–514